Solvent Effects on Molecular and Ionic Spectra. 4. Photochemistry of Fe2+(H2O)6 in Water Revisited: Possible Mechanisms for the Primary Absorption Process Leading to Electron Eject...

ARTICLE *in* THE JOURNAL OF PHYSICAL CHEMISTRY · OCTOBER 1994

Impact Factor: 2.78 · DOI: 10.1021/j100094a015

4 AUTHORS, INCLUDING:

Jinxiu Zeng
University of Sydney
13 PUBLICATIONS **450** CITATIONS
SEE PROFILE

Noel Hush
University of Sydney
310 PUBLICATIONS **12,059** CITATIONS
SEE PROFILE

Jeffrey Reimers
University of Technology Sydney
215 PUBLICATIONS **6,713** CITATIONS
SEE PROFILE

Solvent Effects on Molecular and Ionic Spectra. 4. Photochemistry of $Fe^{2+}(H_2O)_6$ in Water Revisited: Possible Mechanisms for the Primary Absorption Process Leading to Electron Ejection

J. Zeng,[†] J. S. Craw,[†] N. S. Hush,[†,‡] and J. R. Reimers*[,†]

Department of Physical and Theoretical Chemistry and Department of Biochemistry, University of Sydney, NSW 2006, Australia

Received: December 2, 1993; In Final Form: June 20, 1994[⊗]

Our method (parts I−III[1−3]) for estimating solvent shifts of species which have strong specific interactions (e.g., hydrogen bonding) with the solvent is applied to inorganic charge transfer spectra. As the simulation of the structure of ions in solution is not completely straightforward, a number of aspects of the simulation procedure are investigated, concentrating on solvent shift sensitivity. Specifically, we investigate the ultraviolet absorption spectrum of aqueous $Fe^{2+}(H_2O)_6$; for centrosymmetric systems such as this, it is found to be most important to correctly represent the structure of the second coordination shell. Assumptions such as that of rigidity of the inner shell and the particular choice of boundary conditions are of minor consequence. In a process studied extensively over several decades, ultraviolet light absorption results in electron ejection, leading to the photochemical decomposition of water. Several mechanisms for the primary process have been suggested in the past, without consensus being achieved. These include initial metal to ligand charge transfer (MLCT), metallic 3d → 4s absorption, direct electron photodetachment producing a partially solvated electron in a preexisting solvent cavity, and charge transfer to solvent absorption (CTTS). We consider the energetics and solvent shift of the first three of these processes, concluding that the MLCT band is too high in energy, the d → s band could participate, and the photodetachment band is at the correct energy and intensity to account for all that is (as yet) observed of the absorption band. In general, a rather complicated picture of this process in inorganic complexes emerges.

I. Introduction

Electronic absorption spectroscopy has been widely used to investigate the electronic properties of materials, typically in condensed phases. In polar media, a sizeable electrostatic solvent−solute interaction can occur, producing a large solvent (solvatochromic) shift on an electronic absorption band center. Many chromophores, e.g., bisruthenium complexes of aromatics[4−7] and pseudo-one-dimensional wires,[8−10] have complicated structures which are large on the scale of the dimensions of the solvent molecules and often induce some specific solvent−solute interactions. Indeed, such interactions can play a critical role in electron transfer processes in solution.[11] The first papers in this series[1−3,12] developed a method for evaluating the solvent shift appropriate for such situations, particularly if specific interactions such as hydrogen bonds are involved. In these, it was applied to calculate the $^1(n,\pi^*)$ solvent shifts of pyridine and pyrimidine in water. Here we apply this method first to calculate the solvent shift of a localized metal to ligand charge transfer (MLCT) absorption within the inorganic complex $Fe^{2+}(H_2O)_6$ in water and second to estimate the absorption band for photodetachment of an electron from this complex into a preexisting solvent cavity. The results are used to investigate the nature of the primary absorption process involved when this ion acts to photochemically decompose water.

During the past 20 years, many theoretical models have been developed to calculate the solvent shift of electronic absorption band centers. On the basis of Kirkwood's equation,[13] a dipole cavity model, which represents the solute as an electronic-state-dependent polarizable point dipole in a cavity inside a dielectric continuum, has been developed by Onsager,[14] McRae,[15] Bayliss,[16] Lippert,[17] Liptay,[18] Rettig,[19] and others. It has been implemented into quantum mechanical electronic structure calculations, including semiempirical (i.e. intermediate neglect of different overlap (INDO))[20] and *ab initio* (both self-consistent reaction field (SCRF)[21] and multiconfiguration self-consistent reaction field (MCSCRF)[22]) techniques. The cavity shape, however, is always arbitrary and is often taken to be spherical. Recently, Agren and Mikkelsen[23] and Tomasi *et al.*[24] have reviewed the current state of all methods for the calculation of solvatochromic shift. To date, the most complete consideration of all relevant physical effects on an electronic excitation is contained in the microscopic model introduced by Luzhkov and Warshel.[25] However, owing to limitations of computational power currently available, this method is at present only implemented using semiempirical techniques, the applicability of which to intermolecular interactions needs further investigation.

Our method[3] for calculating the effects of a surrounding medium on the electronic properties of a molecule involves two stages: first, standard Monte Carlo or molecular dynamics simulations are performed to determine the equilibrium structure of the solvent around the chromophore in its initial state, and second, sampled configurations are taken and the solvent shift deduced using perturbative expansions of the quantum chemical interactions. This method represents solvent molecules explicitly, and no *arbitrary* parameters are involved. Also, many of the parameters required such as gas-phase charge distributions and polarizabilities may be reliably estimated using standard quantum mechanical techniques. Successful applications of it have been found.[1−3,12]

We use the Monte Carlo method to calculate the structure of a dilute aqueous solution of an inorganic hydrated ion. Recently, Ohtaki and Radnai[26] reviewed all the experimental and theoretical techniques used to investigate the structure and dynamics

[†] Department of Physical and Theoretical Chemistry.
[‡] Department of Biochemistry.
[⊗] Abstract published in *Advance ACS Abstracts,* October 1, 1994.

0022-3654/94/2098-11075$04.50/0

of such complexes. In this work, we do not include counterions explicitly, and hence the sample is not electrically neutral. As a result, the range of ion−water electrostatic interaction is much greater than the size of the sample usually employed (on the order of a 10 Å radius), causing important methodological difficulties in the simulation. Indeed, the treatment of the long-range electrostatic interactions has a significant effect on the calculated radial distribution functions and thermodynamic properties of aqueous solutions.[27−30] Commonly, four different methods are used to treat long-range interactions during simulations: (i) the simple spherical truncation technique, which sets intermolecular interaction equal to 0 for separations larger than some cutoff radius; (ii) smoothing function techniques, which damp the Coulombic interactions to 0 over the outer reaches of the sample; (iii) Ewald summation techniques,[31] which use the periodicity of the system to include the Coulombic interactions at very large distances on the order of many box lengths; and (iv) reaction field techniques,[32] which use a dielectric continuum model of the liquid to evaluate the electrostatic interactions beyond a specific cutoff distance. It is known[28] that, in comparison with results obtained using Ewald summations, simple truncation significantly perturbs the radial distribution functions for quite large distances inside the cutoff radius, while the smoothing function has some, but considerably reduced, effects in that region. For a sample size on the order of that used here, the treatment of the long-range interaction has no significant effect on radial distribution functions (RDFs) in the region within the first 6 Å for monovalent ionic solutions;[30] its influence on the spatial and orientational structure of the solvent around the highly charged solute, however, as well as its effect on the MLCT absorption from the metal to the ligands in the first coordination shell, is not completely known.

Like the choice of boundary conditions, the choice of the intermolecular potential energy surface also has significant effects on the results of simulations of ionic solutions. Because of computational efficiencies, effective pair potentials are often used in such simulations: the key assumption is that many-body interactions and charge transfer effects can be incorporated into effective parameters and evaluated implicitly through the two-body interaction energies. Effective pair potentials between the components of a solution may be generated using an empirical method which fits experimental data such as crystal data, diffraction data, semiempirical calculations, and thermodynamic data using a parametrization of the potential surface. Alternatively, a potential function may be constructed by fitting directly the complete potential surface evaluated from quantum mechanical calculations. This method has the advantage that it does not depend on known experimental data.[33] As Clementi *et al.*[34] first pointed out that the most stable state of a $M^{n+}H_2O$ complex at large separation is actually the charge transfer state, $M^{(n-1)+}(H_2O)^+$, owing to the relative magnitude of the ionization potentials. This is not the case in the liquid state as many-body effects, such as charge transfer and polarization, are very important;[35] an interaction potential determined by fitting the true two-body ion−water potential and used in a liquid state simulation will "attract" excess water molecules into the hydration shell.[36] To remedy this, three-body corrections have been added to the intermolecular potential.[37−40] Recently, Tomasi *et al.*[41] proposed a new method for determining ion−water effective pair potentials which implicitly takes into account both many-body corrections and charge transfer effects: the ion and one water molecule are included inside a dielectric cavity during the electronic structure calculation, known as the self-consistent reaction field (SCRF) technique. Alternatively, true *n*-body potentials may be used to evaluate intermolecular interaction in computer simulations of ionic solutions.[42−44] This technique conceptually simplifies the construction of the interaction potentials, but significantly increases the cost of the computer simulations.

The above approaches aim to generate a potential surface which describes the interactions of the ion both with its ligands in the first coordination shell and with the outer-shell solvent molecules. An alternative suggested by Marcos *et al.*[45] treats the ion and its ligands as a single entity. Its intra-"molecular" potential and its inter-"molecular" potential interaction with the solvent molecules can then be determined independently, considerably reducing demands on *ab initio* computational techniques. The resultant potential surface is considerably more flexible than those which use the same function to describe interactions both inside and outside of the ligand coordination sphere, and pairwise additivity is likely to be a reasonable accurate assumption for the intra-"molecular" interactions. Indeed, potential surface generation becomes particularly simple if one takes the complex to be rigid; using Kollman's[46,47] scheme for potential surface generation, all that is required is a single electronic structure calculation for the complex in the gas phase, possibly requiring the force field to be determined, and reaction fields are not essential. For Marcos's approach to be appropriate, however, ligand to solvent exchange reactions must be slow on the time scale of the phenomena being studied. This is guaranteed for strong binding ligands such as HCN and 2,2'-bipyridyl in aqueous solution, but only applies to aqueous complexes of highly charged ions such as Zn^{2+}, Fe^{2+} and Ru^{2+}. In this paper, we develop such a surface for Fe^{2+} and consider its properties.

During the last 20 years, many experiments have been designed to study solvent effect on the intramolecular electron transfer process in, for example, ruthenium complexes (both with and without aromatic ligands) in aqueous solution.[48] Standard theoretical approaches for such systems involve either *ab initio* or semiempirical SCF/CI or SCRF/CI techniques (see ref 49 and references therein). These methods treat the chromophore explicitly but either ignore the solvent or treat it implicitly as a dielectric continuum. So far, an explicit representation of the solvent around such a complex appears to have been determined only by Broo,[50] using a molecular dynamics simulation. However, he used the same potential to describe interactions both within and outside the ligand coordination sphere, and the potential was derived from a force field calculation. As a consequence, his molecular dynamics simulations predicted that seven water molecules exist in the first coordination shell around Ru^{2+}, as opposed to the six water molecules observed experimentally.[26,51,52] This again emphasizes the importance of the ion−water interaction potential used in the simulations.

Of specific relevance to this work, the general properties of simulations of hydrated ions considered above do indeed apply to hydrated Fe^{2+}. The solvent structure around this ion has been studied for a long time, and several different Fe^{2+}−water interaction potentials have been developed. Curtiss *et al.*[36] constructed an empirical potential from approximate ionic radii and the experimental vibrational frequencies of $Fe^{2+}(H_2O)_6$, as well as a potential from *ab initio* calculations on the Fe^{2+}−H_2O complex. Molecular dynamics simulations showed that the empirical potential produced six water molecules in the first coordination shell, while the *ab initio* potential produced eight. Another Fe^{2+}−water interaction potential constructed by Bertrán *et al.*[53] from *ab initio* data for the monowater complex also produced eight water molecules in the first coordination shell. Many experimental techniques suggest that six water molecules are actually present. Tomasi *et al.*[41] generated a two-body

potential from *ab initio* SCRF potential surfaces of $Fe^{2+}(H_2O)_n$ (n = 1 or 2) complexes, and molecular dynamics simulations using this potential reproduced the experimental coordination number. This appears to be the most accurate currently available. It is clear that many-body contributions do indeed have an important effect on the structure of the solvent.[34]

Other molecular dynamics simulations performed for aqueous Fe^{2+} by Guàrdia and Padró[54] using the empirical potential of Curtiss and either rigid SPC[55] or flexible SPC[56] water models show that the intramolecular motion of water has no significant influence on the ion−water orientation. Hence, all simulations performed herein use rigid water molecules. Note, however, that the above calculations did not allow for the changes in force constants of a water molecule when coordinated in the inner shell; these can cause a significant expansion of the H−O−H equilibrated angle,[57,58] which could affect the structure of the second coordination shell.

The outer-shell electron transfer reaction (i.e., the Fe^{2+}/Fe^{3+} exchange reaction) occurs only in the liquid phase so that the solvent effects on the reaction mechanism are particularly of interest. Newton *et al.* have performed *ab initio* calculations on $Fe^{2+}(H_2O)_6$ and $Fe^{3+}(H_2O)_6$ to study the solvent reorganization[59] and performed molecular dynamics simulations to calculate the solvent isotope effect;[60] Chandler *et al.* have performed classical[61] and quantum[62] Monte Carlo simulations to evaluate the nuclear tunnelling enhancement of the reaction rate.

Another important property of aqueous solutions of Fe^{2+} is their ability to undergo the photochemical reaction

$$2Fe^{2+} + 2H_2O \xrightarrow{h\nu} 2Fe^{3+} + 2OH^- + H_2 \qquad (1)$$

when irradiated at ~250 nm. This process was the subject of considerable research (e.g., refs 63−75) during the 1930s to 1960s, the interest arising from the possible use of this reaction in a solar energy plant. There has been much debate as to the nature of the primary absorption process, with various options including (1) charge transfer absorption of a metal to ligand (MLCT) state localized on one of the ligands[65−67] followed by a subsequent ligand decomposition reaction; (2) d → s absorption producing[70−72] a ^5S state of Fe^{2+} with configuration $3d^5 4s^1$, traditionally thought to be followed by nonradiative transfer of the excitation into a MLCT state and hence to ligand decomposition; (3) a charge transfer to solvent (CTTS) transition[76] in which the electron is excited into a hydrogenic-like orbital over the inner solvent shells, analogous to that observed[77] for halide (etc.) anions, followed by electron ejection and further chemistry; and (4) direct photodetachment to produce a free electron (i.e., an electron lying beyond the first coordination shell in a preexisting solvent cavity,[78,79] partially but not fully solvated),[73,74] followed by reactions of the free electron with water and other species. Note that the expression "charge transfer to solvent" has come to have a colloquial meaning as an umbrella term covering all mechanisms by which an electron is transferred from a chromophore into the solvent's realm. Here, we use this term explicitly with its original and rather technical meaning as described by polaron theory: this process does not change the expectation value of the position of the electron, and the electron is simply placed in a hydrogenic chromophore-centered orbital which permeates out and through the solvent. Motion of the electron's probability center into the solvent happens in a second step after the primary absorption process is complete. This is in contrast to the direct photodetachment mechanism in which the electron's position expectation value moves away from the chromophore into the solution as a result of the primary absorption process, much like as happens in gas-phase photoelectron spectroscopy.

Chemically, the situation is quite complex as the absorption band[63,66,68] (shown later in Figure 8) shows structure, suggesting that more than one of the above processes may be occurring simultaneously. Subsequent to these initial steps, a complex system of chemical reactions ensues (for example, see refs 66,-67,72,80,81), finally resulting in the evolution of hydrogen gas at ca. 8% quantum yield.[72,75] The observation of solvated electrons as reaction intermediates[73,75] indicates that mechanisms 1 and 2, as originally formulated, are incorrect: light absorption leads first to electron ejection, not ligand decomposition. However, the primary step postulated in each of these mechanisms, the MLCT and d → s absorption, are still appropriate, as they could lead to subsequent electron loss. Indeed, the apparent similarity between the observed liquid[63,66,68] and mixed crystal[82] spectra suggests[73] that the observed absorption band is an intrinsic property of the complex, not requiring the presence of a solvent or glass medium. Unfortunately, all these spectra (for example, see Figure 8) terminate mid-band, and so this result is not conclusive.

Somewhat surprisingly, no clear resolution of this fundamental question was reached; this was perhaps partly due to the realization that photooxidation of aqueous ions (etc.) leading to hydrogen gas production is a general phenomenon, not a specific property of the Fe^{2+} system,[68,74,77,83] and a consequent turning of attention to other systems. Over the past few years, advances in femtosecond experimental and quantum simulation techniques have led to the unambiguous characterization of the primary absorption process in a number of systems, and examples of mechanisms 1, 3, and 4 have been characterized. Liquid water, for example, undergoes[84] a two-photon photodetachment (mechanism 4) at energies above 6.5 eV: a 2p electron leaves the chromophore extremely rapidly, localizes still with p angular momentum (as required for a two-photon-allowed process) in a preexisting solvent cavity not far from its source, and there relaxes to produce a solvated electron in its ground s state.[78,79,85−88] Other molecular liquids, such as neat alkanes display similar effects.[89] Alternatively, halide ions[77,90−95] undergo a one-photon allowed p → s CTTS transition (mechanism 3) to produce some short-lived excited complexes and is followed by electron release and capture. This basic mechanism, somewhat modified, has also been observed to apply to neutral chromophores.[96]

Few detailed analyses have appeared for the spectra of inorganic complexes, however. One example is the spectrum of $[Fe(CN)_6]^{4-}$ and related complexes.[74,97−99] These have an intense MLCT band with a long low-frequency shoulder which is believed to be a CTTS transition; absorption at both the band center and shoulder gives rise to electron ejection, suggesting that considerable interaction between the two bands may occur or possibly that more than one mechanism for electron release may be involved. Another example is the $Ru^{2+}(NH_3)_6$ complex,[76] which displays a moderately intense, isolated band which is believed to represent a CTTS transition. The final electronic state is perhaps naively felt[76] to be a hydrogenic 2s orbital, but this is unlikely as this would require a Laporte-forbidden g → g electronic transition. An interesting feature of the photooxidation of inorganic complexes is that the observed absorption intensities appear to vary over 5 orders of magnitude (for example, see refs.[68,74]), suggesting that a variety of mechanisms are involved. Unfortunately, in these examples only part of the absorption spectrum is recorded and estimation of the total intensity may be very difficult: it could well be that these bands in general have considerable structure, with each substructure originating from a different absorption mechanism. Indeed, they often appear as low-frequency tails to other well-characterized bands, and it is possible that mechanisms 3 and 4 could proceed

through vibronic interactions with nearby intense absorption. A recent detailed analysis of the photolysis of $[Fe(CO)_4]^{2-}$ was unable to discriminate between the possible primary absorption mechanisms.[100]

Discrimination between the above mechanisms can be achieved if detailed knowledge of the energetics of each process can be obtained. Of particular importance to mechanisms 1 and 2 is the energy predicted for the postulated primary absorptions of the $Fe^{2+}(H_2O)_6$ complex *in solution*. The internal iron d → s transition involves no substantial charge rearrangement, and hence the solvent shift obtained in taking this complex from the gas phase and dissolving it in water is expected to be quite small, perhaps on the order of a few hundred wavenumbers (our model, which includes electrostatic terms only, predicts no solvent shift at all). If the MLCT transition is delocalized over all of the ligands, then a similar picture would apply; alternatively, if the MLCT transition is localized, it will involve significant charge transfer and hence be expected to show a large solvent shift. Also, as strong hydrogen bonds to the solvent are involved, the solvent shift may be poorly described using dielectric continuum models for the solvent,[3,99] requiring a model such as ours for its evaluation. While much is known about MLCT bands when the acceptor orbital is a low-lying ligand π orbital, little is known about such bands when the transfer is to a σ orbital, as the band center of such a transition lies in the vacuum ultraviolet region of the spectrum. Simple energetic considerations indicate that mechanisms 3 and 4 are plausible.[73,74] From the standard reduction potentials[101,102] of Fe^{2+}/Fe^{3+} and e_g^-/e_{aq}^-, ΔG for the process of transferring an electron from equilibrated Fe^{2+} to produce equilibrated Fe^{3+} and an isolated solvated electron is 3.54 eV; corrections for entropy changes[101,103] for this process give the estimated energy of the absorption origin at $\Delta H = 4.04$ eV, at the foot of the observed[63,66,68] absorption band.

Our objectives in this work are 2-fold: first, we perform electronic structure and liquid structure simulations and spectroscopic calculations for mechanisms 1, 2, and 4, investigating the nature of the photochemical processes of aqueous Fe^{2+}; and second, we seek to determine general principles for the determination of solvent shifts of inorganic complexes and concentrate on determining the aspects to which the solvent shift is most sensitive. Section II describes all of the potential surfaces used as well as other variations used during the simulation of the liquid structure. It also describes the algorithms used in order to determine the MLCT (mechanism 1) and photodissociation (mechanism 4) solvent shifts from the liquid structure. In section III, results are given for the MLCT solvent shift, relating it closely to results for the solvent structure and specific issues which arise for this type of calculation. Section IV focuses on the mechanism of the photochemical process. Both INDO/S and *ab initio* calculations are performed for the energy of the MLCT and d → s bands in the gas phase, allowing the absolute solution absorption band center to be predicted. Further, the absorption spectrum for the direct photodetachment, mechanism 4, is calculated and compared to the experimental spectrum.

II. Computational Detail

(a) Monte Carlo Simulations. Constant pressure, density, and temperature (NPT ensemble)[104] and constant volume, density, and temperature (NVT ensemble) Monte Carlo[105,106] simulations of a single Fe^{2+} ion in a solution of 190 rigid water molecules are performed at a temperature of 298 K with periodic boundary conditions. The NPT ensemble simulations are performed at 1 atm of pressure, while the NVT ensemble simulations are performed at a density of 1 g/cm^3. To accelerate convergence of the simulations,[107] solute displacements and volume changes are performed every 10 and 100 moves, respectively. The magnitude of the Monte Carlo displacements are adjusted to maximize the diffusional and rotational motions (only about 25% of all moves are accepted), and solvent molecules are selected for displacement with a probability proportional to the solute–solvent separation.[107] Equilibration is performed for at least 5×10^6 moves, and an ensemble of 5×10^6 configurations is then generated. Evenly spaced configurations (5×10^3) are selected and their properties averaged in order to determine the ion–water radial distribution functions (RDFs), and 500 equally spaced configurations are stored for subsequent orientational and spectral analysis.

(b) Boundary Conditions. Simulations are performed using a variety of boundary techniques, with the aim of finding the simplest and easiest to use, which adequately reproduce the solvent structure and MLCT solvent shift. The following methods are used: ST, simple truncation technique in the NPT ensemble; SM, smoothing function technique in the NPT ensemble; EWV, Ewald summation technique in the NVT ensemble; and EWP, Ewald summation technique in the NPT ensemble.

Method ST involves a simple truncation of the cutoff interaction potential at the radius R_C of the inscribed sphere of the unit cell ≈ 9.5 Å. This is modified slightly in method SM, in which a smoothing function[108]

$$S(r_{Fe-O}) = \begin{cases} 1, & r_{Fe-O} \le r_1 \\ C_0 + C_1\delta^3 + C_2\delta^4 + C_3\delta^5, & r_1 \le r_{Fe-O} \le r_c \\ 0, & r_{Fe-O} \ge r_c \end{cases} \quad (2)$$

where $\delta = r_{Fe-O} - R_L$, is used to damp the interaction potentials to 0 in the region $(R_C - R_L) = 3$ Å inside the cutoff radius R_C. The coefficients C_0, C_1, C_2, and C_3 are chosen to make the smoothing function and its first two derivatives continuous at R_L and R_C and are given by

$$C_0 = 1 \qquad C_1 = \frac{-10}{(R_C^2 - R_L^2)^3} \quad (3)$$

$$C_2 = \frac{15}{(R_C^2 - R_L^2)^4} \qquad C_3 = \frac{-6}{(R_C^2 - R_L^2)^5}$$

For the SM and ST methods, we use periodic truncated octahedral boundary conditions,[109–111] and the cutoff radius corresponds to the distance from the center to the nearest (111) face of the unit cell. NPT ensemble simulations are used, and hence this radius fluctuates. The other two calculation methods use the Ewald summation technique. They differ in that EWV uses the NVT ensemble simulation with periodic cubic boundary conditions, while EWP[112] uses the NPT ensemble with periodic truncated octahedral boundary conditions. We use the minimum image convention for the Ewald summations in real space.[113] Also, a neutralizing background[114,115] is used to solve the convergence problems created by the ion self-energy term, although we find Pettitt *et al.*'s[116] suggestion that this term can be completely ignored to be quite accurate for the properties considered.

(c) Potential Surfaces. Five different potential surfaces are used in the simulations with the aim of determining the simplest method possible for the construction of potential surfaces for this type of problem. They are TF1, Tomasi's[41] potential surface for *all* water molecules (there is thus a flexible inner shell); TR, Tomasi's[41] potential for outer-shell waters with a rigid inner shell; TF2, Tomasi's[41] potential for outer-shell waters with a

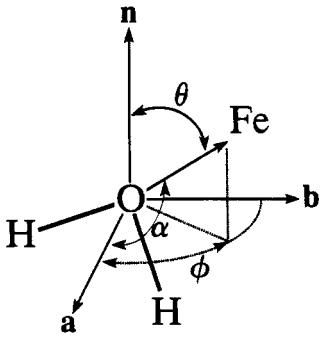

Figure 1. Polar angles θ and ϕ used in the construction of the intramolecular component of potentials TF2 and EF, and the tilt angle α used in the structural analysis. Here, **a**, **b**, and **n** are the dipole, in-plane, and normal vectors of the water molecule, respectively.

force field to describe the interactions of the ion with its inner shell; ER, a hydrated ion potential derived herein with a rigid inner shell; and EF, a hydrated ion potential derived herein with a flexible inner shell whose potential is described using a force field.

In all cases, the SPC water potential is used to describe the interactions between *all* water molecules. These molecules are held rigid in all simulations.

The force field used to describe the interaction between the ion and each ligand in potentials TF2 and EF is

$$V = \frac{1}{2}k_r(r - r_e)^2 + \frac{1}{2}k_\theta(\theta - \theta_e)^2 + \frac{1}{2}k_\phi(\phi - \phi_e)^2 \quad (4)$$

The geometrical variables θ and ϕ are defined in Figure 1; they are the polar coordinates which describe the O—Fe vector in the reference frame of the water molecule with r the O—Fe distance, θ the angle between the O—Fe vector and the vector normal to the water plane, and ϕ the angle between the water dipole vector and the O—Fe vector projected onto the plane of the water molecule. Note that the ion−water potential is not a function of the angle of rotation of the water molecule around the O—Fe vector due to the cylindrical symmetry of the interaction. In eq 4, r_e, θ_e, and ϕ_e are parameters describing the equilibrium geometry, and k_r, k_θ, and k_ϕ are force constants. Their values are obtained by examining Tomasi's potential surface[41] for the $Fe^{2+}H_2O$ cluster, selecting the parameters so as to reproduce its structure and force constants; values obtained are $r_e = 2.09$ Å, $\theta_e = 90°$, $\phi_e = 180°$, $k_r = 163$ kcal/(mol Å^2), $k_\theta = 30$ kcal/(mol rad^2), and $k_\phi = 58$ kcal/(mol rad^2).

In the TR potential, the inner shell is held rigidly at the above T_h equilibrium geometry. Alternative structures are possible, however, for example, a D_{3d} structure is also a local minimum on Tomasi's surface and lies just 1.3 kcal/mol higher in energy than the T_h structure.

We generate our own potential surfaces ER and EF on the basis of Marcos's approach,[45] which treats the ion and its six water ligands as a single molecular species. The interactions of this complex with the solvent are determined using Kollman's scheme for the generation of the intermolecular potential surfaces. It is

$$V = V_C + V_{LJ} \quad (5)$$

where V_C is the Coulombic interaction between all 19 atomic charges on the $Fe^{2+}(H_2O)_6$ complex and all $3 \times 184 = 552$ atomic charges on the solvent water molecules,

$$V_C = \sum_{i=1}^{19}\sum_{j=1}^{552}\frac{q_i q_j}{r_{ij}} \quad (6)$$

and V_{LJ} is the Lennard-Jones interaction of the oxygen atoms of the six ligand water molecules with those of the 184 solvent molecules,

$$V_{LJ} = \sum_{i=1}^{6}\sum_{j=1}^{184}4\epsilon[(\sigma/r_{ij})^{12} - (\sigma/r_{ij})^6] \quad (7)$$

Note that, as the ligands effectively prevent solvent molecules from approaching too close to the ion, no Lennard-Jones interactions between the ion and the outer-shell water molecules are necessary. For the water molecules, the values of the atomic charges and Lennard-Jones parameters are taken from the values used in the SPC potential for the solvent−solvent interactions; these are $q_O = -0.82e$, $q_H = 0.41e$, $\epsilon = 0.1554$ kcal/mol, and $\sigma = 3.165\,56$ Å. For the hexaaquo complex, we obtain a gas-phase atomic charge distribution from the electrostatic potential (ESP) obtained from an *ab initio* electronic structure calculation at an assumed[51] equilibrium geometry of $r_e = 2.12$ Å, $\theta_e = 90°$, and $\phi_e = 180°$ (i.e., T_h symmetry). This is performed using the multiconfigurational self-consistent field (MCSCF) technique with an effective-core-potential basis set for iron[117] and oxygen atoms[118] and a double-ζ basis set for hydrogen[119] via the HONDO[120] suite of programs. The atomic charges are fitted at data points equally spaced in the region from 1.4 to 2.5 van der Waals radii of the complex, which are taken for iron, oxygen, and hydrogen atoms to be 0 (the oxygen atoms prevent close approach to the central atom), 1.52, and 1.2 Å, respectively. The deduced charges on the complex are $q_{Fe} = 1.5326e$, $q_O = -0.9765e$, and $q_H = 0.5272e$, indicating that ligand charge transfer and polarization effects are important.

The potential ER is obtained by assuming that the complex is rigidly held at its equilibrium geometry. EF differs from this potential only in that the first coordination shell is allowed to relax, and a function of the form of eq 4 is used to describe the Fe−ligand interactions. The parameters in this function are obtained by determining *ab initio* the force constants for the $Fe^{2+}(H_2O)_6$ complex and fitting these numbers to the total potential obtained by combining the six interactions of eq 4 with the water−water SPC potential. The results are $k_r = 216$ kcal/(mol Å^2), $k_\theta = 30$ kcal/mol, and $k_\phi = 112$ kcal/mol. Note that the *ab initio* ligand stretch frequency is calculated to be 401 cm^{-1}, in satisfactory agreement with both the observed value of 380 cm^{-1} and the value obtained from Tomasi's potentials (both TF1 and TF2) of 390 cm^{-1}.

A summary of all the simulations actually performed is given in Table 1. Note that they are named according to the boundary conditions and the potential function used.

(d) Localized MLCT Solvent Shift Evaluation. In evaluating the MLCT solvent shift, we treat the $Fe^{2+}(H_2O)_6$ complex as a *single* chemical species, evaluating the change in its MLCT absorption frequency when it is transferred from the gas phase to solution. We assume that the transition is localized (i.e., to only one of the six ligands) and that an entire electron is transferred from the iron to the oxygen atom of the water molecule. Breakdown of these assumptions will result in the actual solvent shift being smaller in magnitude than the one which we calculate: we aim to determine a possible *lower bound* to the absorption frequency. Two major contributions to this solvent shift occur, a direct effect due to the solvation of the chromophore and an indirect effect arising from fluctuation and distortions of the geometry of the complex. We assume that the structural changes of the inner shell have no significant effects on the transition energy and calculate the solvation term only. This is performed by sampling liquid configurations from the Monte Carlo calculations and calculating, using our perturbative model,[3] detailed electrostatic interaction energies between

TABLE 1: Description of the Eight Monte Carlo Simulations Performed[a]

	simulation							
	TF1/ST	TF1/SM	TF1/EWV	TF1/EWP	TF2/SM	TR/SM	ER/SM	EF/SM
ensemble	NPT	NPT	NVT	NPT	NPT	NPT	NPT	NPT
boundary condition	simple truncation	smoothing function	Ewald sum	Ewald sum	smoothing function	smoothing function	smoothing function	smoothing function
unit cell	TO	TO	cubic	TO	TO	TO	TO	TO
solute	Fe^{2+}	Fe^{2+}	Fe^{2+}	Fe^{2+}	$Fe^{2+}(H_2O)_6$	$Fe^{2+}(H_2O)_6$	$Fe^{2+}(H_2O)_6$	$Fe^{2+}(H_2O)_6$
solute−solvent potential	Tomasi	Tomasi	Tomasi	Tomasi	Tomasi	Tomasi	ESP	ESP
ion−ligand potential	Tomasi	Tomasi	Tomasi	Tomasi	force field	rigid	rigid	force field

[a] TO, periodic truncated octahedral unit cell; cubic, periodic cubic unit cell; Tomasi, the Fe^{2+}−water interaction potential generated by Tomasi.[41]

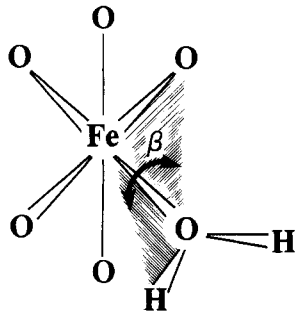

Figure 2. Torsional angle β between an O—Fe—O plane and an Fe—O—H plane used in analyzing the structure of the inner coordination shell.

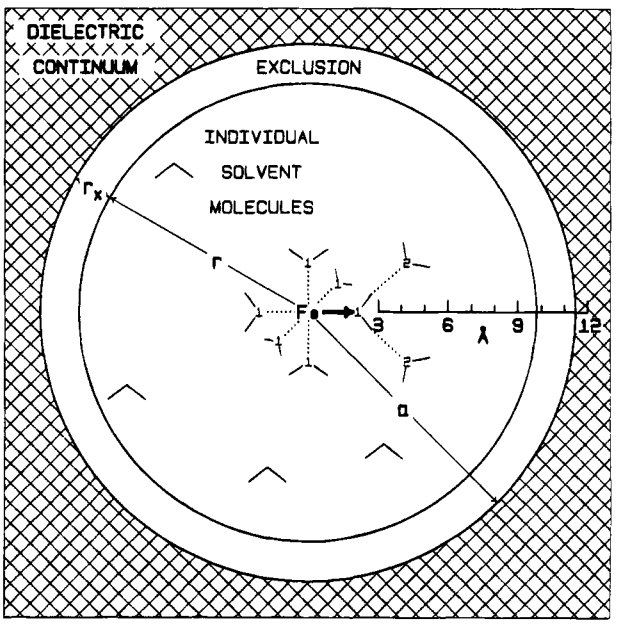

Figure 3. Key features of the solvent-shift model including the dielectric continuum, the exclusion layer, some of the individually represented solvent molecules, the central iron atom, and a length scale typical of the calculations, as well as an arrow which represents the metal to ligand charge transfer (MLCT) process. The water molecules marked "1" are those located in the first coordination shell around Fe^{2+}, while those marked "2" are the water molecules hydrogen bonded to the postulated charge-acceptor water molecule.

the $Fe^{2+}(H_2O)_6$ complex and the remaining water molecules. Key features of the method are shown in Figure 3; the six water molecules of the complex are labeled "1". The complex and every solvent water molecule whose oxygen atom lies within a radius r of it are enclosed within a small excluded volume of radius r_x and then inside a dielectric continuum of radius $a = r + r_x$. The exclusion radius r_x prevents unphysically large interactions across the boundary and must exceed 1.0 Å, the OH bond length in SPC water; we set it to 1.001 Å. Practically, r cannot be so small as to exclude the complexed water molecules, and it cannot be so large as to exceed the unit-cell inscribed-sphere radius; here, we find that 3.2 Å $< a <$ ~10.5 Å. The dielectric constant, refractive index, and isotropic polarizability of water are taken[121,122] to be $\epsilon = 78.5$, $n = 1.333$, and $\alpha = 9.6164$ au, respectively. As the electrostatic interactions used in the solvent shift evaluation are n-body interactions of polarizable water molecules, the solvent water atomic charges are set to $0.33e$ and $-0.66e$ for hydrogen and oxygen atoms, respectively, so as to reproduce the observed dipole moment of gas-phase water.[121] In the same spirit, the central ion is assigned a charge of $+2e$ in the ground electronic state; we performed trial calculations in which charge transfer from the metal to the ligands in the excited state is included, and these

indicate that the initial ion charge is not a critical parameter. The localized electronically excited state is represented by transferring an electron from iron to one of the ligand water molecules, as shown in Figure 3; this is presumably an overestimate of the actual charge transfer, and hence our results should overestimate the magnitude of the actual solvent shift. No polarizability center is located on the bare Fe^{2+} ion in either its initial or final states, as polarization of the wave function of the hydrated cation has been shown to be relatively small.[123] All water molecules are treated as polarizable, however, and hence the hexaaquo complex is polarizable. A consequence of this is that a nonzero value is calculated for the solvent shift of the isolated complex in the gas phase due to the electrostatic interactions within the complex itself. This term is, of course, just one of many contributions to the gas-phase transition energy, and we subtract this energy from all calculated solvent shifts.

(e) Simulation of the Photodetachment Spectrum. According to postulated mechanism 4, the absorption spectrum arises from the direct photodetachment of an electron from the metal to a preexisting cavity in the solvent lying beyond the ligand coordination shell. In the gas phase for a bare Fe^{2+} ion, this process is observed and the ionization energy is known[124] to be 30.64 eV. In solution, a process of this type undergoes an enormous solvent shift (later, we calculate ca. −30 eV or −240 000 cm^{-1}), principally due to the differences in the solvation energy of the di- and trivalent ion, and our method for evaluating solvent shifts may be applied for this process. We proceed by examining a liquid structure, determining the location of all solvent cavities, sequentially transferring an electron from the ion to each of these cavities, and determining the change in the electrostatic energy. Cavities are isolated by searching for locations which maximize the distance to the closest oxygen atom, and a cavity radius r_c is defined to be the average of all the distances from the center to the oxygen atoms of the water molecules in its first coordination shell; other definitions are possible.[78]

Account must also be taken of the kinetic energy of the electron when it is confined to lie in a solvent cavity. This quantity has been calculated by quantum simulations of the equilibrated solvated electron[125,126] and found to be 2.2 eV at 298 K. The equilibrated structure has 6-fold coordination of water around the electron and has an average electron−oxygen separation of 3.3 Å. Both diffuse (electron in a dielectric continuum) and confined (particle in a box) models for a solvated electron indicate that its kinetic energy increases proportional to the square of the reciprocal cavity size, and hence we assume that the kinetic energy is given by

$$E_K = (3.3/r_c)^2 \times 2.2 \text{ eV} \tag{8}$$

where r_c is in angstroms.

Another contribution to the transition energy is the exchange repulsion between the solvated electron and the electrons bound within the solvent molecules. In general, the effects of these interactions are believed to be small provided that the electron does not approach the atoms too closely,[78,125-127] and the solvated electron has been likened to a F^- ion. We assume that the exchange repulsion can be represented using a hard-sphere potential, the consequence of which is that cavities are only considered if they lie no closer that 2 Å to any oxygen atom. Note that this criterion effectively eliminates any cavity which lies within the first coordination shell of the ion. The transition energy producing an electron located in a preexisting solvent cavity is thus given by

$$h\nu = 30.64 \text{ eV} + E_K + h\Delta\nu \tag{9}$$

where $h\Delta\nu$ is the solvent shift.

In order to estimate the intensity and width of the absorption band, we postulate that intensity arises from only direct through-space electron transfer and estimate the transition moment for this process. The initial state $|\psi_i\rangle$ of the electron is a totally symmetric linear combination of the three metal t_{2g} orbitals, and we represent this simply as an iron 3s Slater orbital whose exponent is taken to be that of the iron 3d orbitals as adopted by Zerner,[128,129] 2.6 au. Using the analogy between the solvated electron and a F^- ion,[78] we represent the final state of the electron $\langle\psi_f|$ using a fluorine 2s Slater orbital, whose exponent[129,130] is also 2.6 au. The one-electron matrix element coupling these two states is given in semiempirical theories[130] as

$$V = \frac{-q_f S}{r_{Fe-el}} \times 14.4 \text{ eV} \tag{10}$$

where r_{Fe-el} is the cavity center to ion distance in angstroms, $S = \langle\psi_i|\psi_f\rangle$ is the overlap of the two Slater orbitals, and $q_f = 3e$ is the charge of the final state of the ion. Perturbation theory then gives the transition moment as

$$M = (V/h\nu) r_{Fe-el} \tag{11}$$

which is evaluated, leading to the calculation of the absorption spectrum. Note that this method ignores contributions to the width of the absorption band arising from Franck−Condon displacements of the water molecules around the ion between the initial and final electronic states.

III. MLCT Solvent Shift and the Solvent Structure

Although a variety of potential functions and boundary conditions are used in different simulations (see Table 1), we find that most variants give rise to qualitatively similar results for the solvent structure and solvent shift. First, in an overview, we proceed by considering just one variant, use of the smoothing function SM combined with Tomasi's potential TF1 (we call this simulation TF1/SM), concentrating on the major qualitative features of the results. Later, we examine the results of other simulations in the context of specific issues which arise.

(a) Overview. *(i) Structure.* The radial distribution functions $g_{Fe-O}(r)$ and $g_{Fe-H}(r)$ obtained from the TF/SM simulation are shown in Figure 4 and indicate that there exists a well-defined first coordination shell in the region 1.9 Å < r < 2.4 Å. The maximum of the peak in $g_{Fe-O}(r)$ is at 2.12 Å, and the coordination number is 6, both in agreement with experimental results[51] and other simulations.[41] A second peak in the region 3.5 Å < r < 5.0 Å indicates that a second coordination shell can be isolated, and integration of g_{Fe-O} shows that there are ca. 12 water molecules in this shell. This is in agreement with experimental measurements[26] and theoretical analysis.[36,41,54] Beyond 5 Å, the structure is sensitive to the boundary conditions, as discussed in section IIIb.

The orientational structure of the water molecules around the ion is represented in terms of the tilt angle α between the dipole vector of a water molecules and the Fe^{2+}−oxygen bond vector, as illustrated in Figure 1. The total ion−water electrostatic energy may be expressed in terms of $\langle\cos\alpha\rangle(r)$ as

$$V_{el} = 4\pi\varrho q_{Fe}\mu_w \int_0^\infty \langle\cos\alpha\rangle(r)\, g_{Fe-O}(r)\, dr \tag{12}$$

where $\langle\cos\alpha\rangle(r)$ is the average value of cos α for water molecules at ion−oxygen separation r, ϱ is the average liquid density, q_{Fe} is the charge on the ion, and μ_w is the dipole moment of a SPC water molecule. Results for $\langle\cos\alpha\rangle(r)$ are given in Figure 4; for the first coordination shell (1.9 Å < r < 2.4 Å),

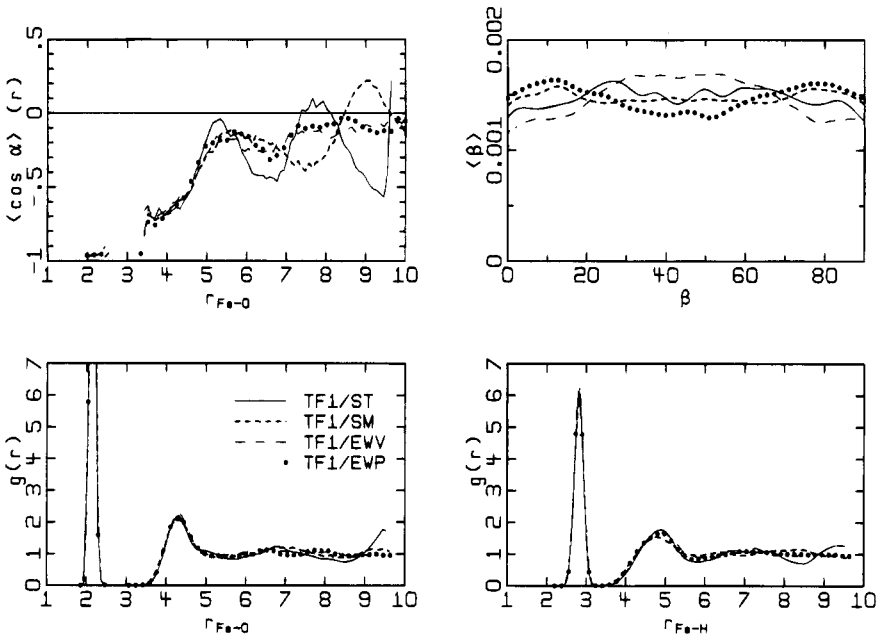

Figure 4. Liquid structure obtained using Tomasi's potential[41] TF1 and four different boundary conditions: ST, simple truncation; SM, smoothing function; EWV, Ewald summation in the NVT ensemble; EWP, Ewald summation in the NPT ensemble. The structural properties shown are the radial distribution functions for iron with oxygen and iron with hydrogen, the distance dependence of the orientation structure $\langle \cos \alpha \rangle(r)$ where α is the tilt angle between the $\mathbf{r}_{O-Fe}$ vector and the dipole vector of water molecule, and the probability (per degree) of occurrence of the innershell interwater torsional angle β between an O—Fe—O plane and the connected Fe—O—H plane; see Figure 2.

$\langle \cos \alpha \rangle$ is close to -1, reflecting the controlling effect of the ion on the orientation of these water molecules and the overall stereochemistry;[131] specifically we obtain $\langle \alpha \rangle = 164°$. This tilt angle has been measured in mixed crystals[57] and concentrated aqueous solutions[26,132] using several different experimental techniques. For highly concentrated solutions, it is found that $\langle \alpha \rangle = 148° \pm 15°$, arguably smaller than our prediction for dilute solutions. Neutron and X-ray diffraction studies[133] on Ni^{2+} solutions show that $\langle \alpha \rangle$ is concentration dependent and decreases at high concentration; for Ni^{2+}, they predict that $\alpha = 180° \pm 20°$ at low concentration, and hence our results are quite plausible. In Figure 4, there is a discontinuity in $\langle \cos \alpha \rangle$ between 2.4 and 3.5 Å, as the first and second coordination shells do not overlap significantly. From 3.5 to 4.4 Å , there is a slow but definite increase in $\langle \cos \alpha \rangle$. The orientational effect remains important beyond the first coordination shell, as seen previously in molecular dynamics simulations.[54]

Further details of the relative orientational structure of water molecules within the inner coordination shell are described in terms of the angle β shown in Figure 2. This is the angle between an O—Fe—O plane (here, the oxygens must be related *cis*) and an Fe—O—H plane. The probability of occurrence of angle β, $\langle \beta \rangle$, is shown in Figure 4; we see that all angles have similar probability, indicating that little intra-first-shell-water correlation exists. To determine the cause of this, we first quenched some of the liquid configurations to $T = 0$ K and found that the broad angular distribution remained. Next, we considered the isolated $Fe^{2+}(H_2O)_6$ complex and determined its structure using Tomasi's potential TF1 at $T = 0$ K. The result was an ordered structure of T_h symmetry in which all torsional angles are 0° or 90°. Finally, we determined the structure of this complex surrounded by just its second coordination shell, i.e. $Fe^{2+}(H_2O)_{18}$. The distribution of $\langle \beta \rangle$ at 0 K is very broad, reminiscent of that found for both the original and quenched liquids. Hence, we conclude that the central ion has only a minor role in characterizing β, this variable being determined primarily by interaction with the surrounding fluid.

(ii) MLCT solvent shift. The direct effects of solvation on the electronic excitation of the chromophore consist of two contributions: one from the specific interaction between the chromophore and explicit solvent molecules and one from nonspecific long-range dielectric solvation. Long-range dielectric solvation dominates the solvent shift if a long-distance charge transfer process is involved, while the specific interaction effects become important when a hydrogen bond between the chromophore and the solvent is disturbed.[3] Key features of the electronic absorption process are shown in Figure 3, where the six inner-shell water molecules are labeled "1". The absorption is assumed to take an electron from the ion to just one of these water molecules, breaking its hydrogen bonds to its neighboring water molecules, labeled "2", in the second coordination shell. As a result, a blue contribution to the solvent shift is expected.[134] Interactions with the solvent water molecules other than those two are regarded as describing the effects of the dielectric solvation of the chromophore dipole. In systems involving long-distance electron transfer, the donor (here Fe^{2+}) and acceptor (here H_2O) could be considered to lie in *separate* solvent holes. The solvent shift thus expected would be given by

$$\Delta\nu = \frac{\epsilon - 1}{\epsilon} \sum_{\text{holes}} \frac{-q_i(q_f - q_i)}{a} \tag{13}$$

where a are the hole radii, ϵ is the dielectric constant, and q_i and q_f are the charges inside each hole in its initial and final states, respectively. For the bare Fe^{2+} ion a value of $a = 2$ au would result in $\Delta\nu = -1$ au or $-220\,000$ cm^{-1}, a huge red shift. Such a model may be appropriate for a photodetachment transition, but it is not appropriate here for the MLCT transition, as both the Fe^{2+} and H_2O really reside in the *same* solvent hole. Treating the charge transfer from Fe^{2+} to H_2O in the same solvent hole simply as a change $\Delta\mu$ in a point dipole μ_g located at the cavity center, the solvent shift is given by[18,19]

$$\Delta\nu = -\frac{2(\epsilon - 1)}{2\epsilon + 1} \frac{1}{a^3} \mu_g \Delta\mu - \frac{(n^2 - 1)}{(2n^2 + 1)} \frac{1}{a^3} \Delta\mu^2 \tag{14}$$

where n is the solvent's refractive index. Our chromophore is now the hexaaquo ion, and we put $a = 3.2$ Å, $\mu_g = 0$, $\Delta\mu =$

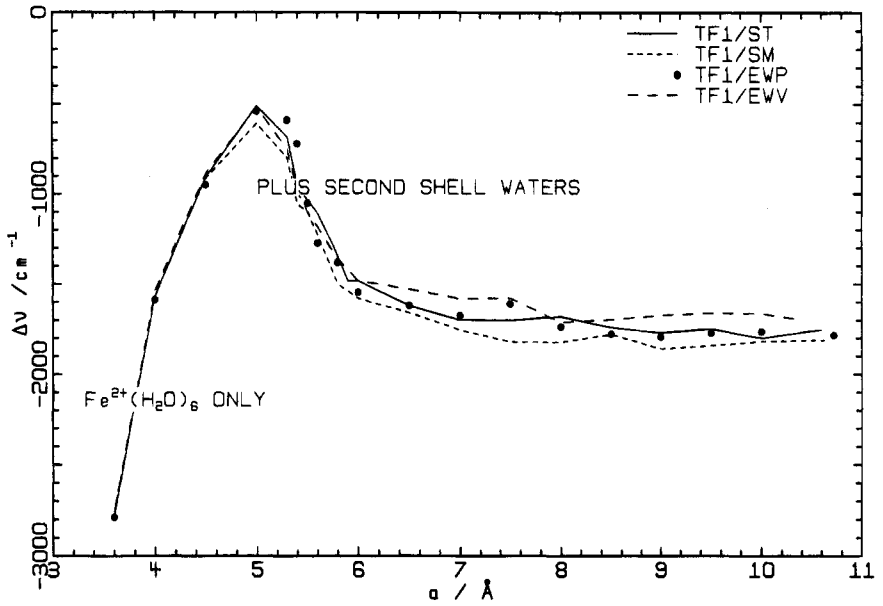

Figure 5. MLCT solvent shift $\Delta\nu$ is shown as a function of the outer cavity radius $a = r + r_x$ (at exclusion radius $r_x = 1.001$ Å) obtained using Tomasi's potential TF1 and various boundary conditions: ST, simple truncation; SM, smoothing function; EWV, Ewald summation in the NVT ensemble; EWP, Ewald summation in the NPT ensemble.

2.12 eÅ, $\epsilon = 78.5$, and $n = 1.333$, predicting $\Delta\nu = -2700$ cm^{-1}. This is really quite a small value on the scale of solvent shifts expected for charge transfer transitions and arises because the dipole moment of the ground state μ_g is 0. The contributions to the solvent shift arising from specific bonding effects and from dielectric solvation effects are expected to be of *opposing* signs, and the net effect may be even more anomalously small.

Results actually obtained for the TF1/SM simulation are given in Figure 5. There, the outer cavity radius a is expanded from a value so small that no explicit water molecules are included inside to the maximum radius permitted by the 190-molecule simulation, and the solvent shift is plotted as a function of this radius. Below $a = 5$ Å ($r_{Fe-O} = 4$ Å), no explicit water molecules outside the inner coordination shell are included, and the solvent shift shows the $1/a^3$ dependence expected from eq 14; its magnitude is significantly enhanced, however, due to the inclusion of polarizability centers within the solute complex.[18] Between 5 Å $< a <$ 6 Å (or 4 Å $< r_{Fe-O} <$ 5 Å), the water molecules in the second coordination shell are explicitly included, and the magnitude of the solvent shift increases considerably. Beyond this radius, very little change to the solvent shift occurs, indicating that it is insensitive to the long-range solvent structure. We see from eq 12 that the ion−water energy is a function of $\langle\cos\alpha\rangle(r)$, and, as for the TF1/SM simulation, this function oscillates at large r (see Figure 4); a similar oscillation of the solvent shift with increasing a would naively be expected. The interaction of importance here, however, is actually the interaction between the change in the dipole $\Delta\mu$ of the chromophore and the water dipoles, and, as the ground state equilibrium structure is isotropic at long range with respect to the orientation of the chromophore dipole, this term averages to 0, independent of the solvent structure. It corresponds to the first term in eq 14. The main long-range contributions to the solvent shift arise from the polarizability of the water molecules, and as we have taken this to be isotropic, this term is also independent of the tilt angle α.

The solvent shift is thus dominated by the second coordination shell, and, within this shell, contributions from both specific hydrogen bonds and from dielectric solvation occur. To determine the relative contributions of each, we performed two solvent-shift calculations each with a set to the maximum value, but containing different numbers of water molecules. In the first calculation, only the two water molecules labeled "2" in Figure 3 are included as the solvent, and the remaining 182 solvent molecules are excluded. This produces a solvent shift of +6000 cm^{-1}. In the second calculation, these two solvent molecules are excluded and the remaining 182 included, producing a solvent shift of −7600 cm^{-1}. As the solvent shift evaluated using all 186 solvent molecules is −1800 cm^{-1}, removing the two hydrogen-bonded molecules modifies the solvent shift by −5800 cm^{-1}, slightly larger than the value expected based on the first calculation, as the polarization energies involved are not additive. Nevertheless, we see that hydrogen-bonding effects account for a blue shift of about 5900 cm^{-1}, but this is opposed by a red shift of about 7700 cm^{-1} arising from dielectric solvation, and the net solvent shift is quite small.

(b) Effects of Varying the Boundary Conditions. Simulation results obtained using Tomasi's potential[41] with four different sets of boundary condition, TF1/ST, TF1/SM, TF1/EWV, and TF1/EWP, are shown in Figure 4. For the radial distribution functions $g_{Fe-O}(r)$ and $g_{Fe-H}(r)$, our TF1/EWV calculation reproduces the results previously obtained from molecular dynamics simulations.[41] All four methods produce qualitatively similar results, with the exception of TF1/ST, which generates a sharp peak around the boundary. Similar effects have also been observed in simulations of monovalent ions.[30] Significantly, the spatial structure of the solvent in the first and second hydration shells are *independent* of the boundary condition used.

The orientational structure $\langle\cos\alpha\rangle(r)$ is independent of the boundary conditions used throughout the first and second coordination shells and slightly beyond, up to about $r = 6$ Å. Beyond this, the simulations performed using Ewald summations produced little change in the orientational structure, which becomes random (i.e., $\langle\cos\alpha\rangle$ approaches 0), as expected for bulk liquid outside the sphere of influence of the ion. Qualitatively similar results for this function have been observed in other simulations.[54] Large oscillations beyond ~5 Å occur when the simple truncation boundary condition ST is used, with the effects seen in the radial distribution functions being amplified. The smoothing function SM damps these oscillations considerably, with their onset being delayed to $r = 7$ Å.

The probability distribution functions for the torsional angle

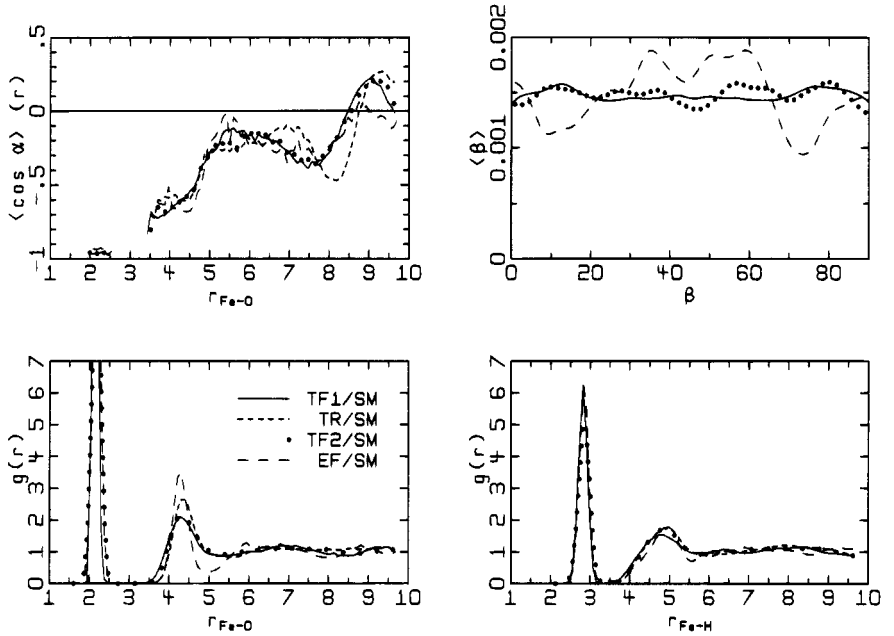

Figure 6. Liquid structure (see Figure 4) obtained using the smoothing function SM and four different potential surfaces: TF1, Tomasi's potential, flexible inner shell; TR, Tomasi's potential for outer-shell interactions with a rigid inner shell; TF2, Tomasi's potential for outer-shell interactions with a force field for the inner-shell interactions; and EF, our ESP-derived potential for the outer-shell interactions with a force field for the inner-shell interactions.

β show qualitatively similar behavior independent of the boundary conditions used: this variable appears to be almost uniformly distributed. Quantitatively, however, discernible differences do occur, and we see that some properties of even the inner coordination shell are effected by the boundary conditions, applied some 8 Å away!

The consequence of changes in boundary conditions, which is of primary interest to us here is the possible change of MLCT solvent shifts. The solvent shift evaluated as a function of cavity radius is plotted for all four boundary conditions in Figure 5, the asymptotic limits being -1750, -1810, -1690, and -1780 cm^{-1} for the TF1/ST, TF1/SM, TF1/EWV, and TF1/EWP simulations, respectively. Although the boundary conditions do effect the liquid structure, they have only a minor effect on the calculated solvent shift. This occurs because the solvent shift is determined essentially by the second coordination shell (molecules with $r < 5$ Å and hence $a < 6$ Å), and the solvent structure in this region is determined in detail quite accurately independent of the boundary conditions used. Note that, as mentioned earlier, even though the boundary conditions used in TF1/ST and TF1/SM lead to oscillations in the spatial and orientational structure of the solvent, they do not lead to similar oscillations in the solvent shift.

(c) Use of a Rigid Inner Coordination Shell. We have seen in Figure 4 that the inner coordination shell has a well-defined radial and tilt angle structure, as exemplified by $g_{Fe-O}(r)$ and $\langle \cos \alpha \rangle(r)$, and a near random torsional structure, as exemplified by $\langle \beta \rangle$. If this structure can be held rigid, then it is much easier to generate the required intermolecular potential surfaces. Figure 6 shows results obtained using the one set of boundary conditions, the smoothing function SM, and a variety of potential functions including TF1, TR, and TF2, which differ only in the treatment of the interactions of the ion with its inner coordination shell. Potential TF1 uses Tomasi's[41] full potential surface and is the reference calculation; the other two surfaces are approximations to this surface, and we examine how well they reproduce the structural and spectroscopic properties.

In simulation TR/SM the $Fe^{2+}(H_2O)_6$ complex is kept rigid. The resulting radial distribution function g_{Fe-O} shown in Figure 6 indicates that the second coordination shell is more structured than that in the reference simulation TF1/SM. The orientational structure $\langle \cos \alpha \rangle(r)$ is not effected greatly, however, although the unphysical oscillations out near the cell boundary distort somewhat. Nevertheless, as the solvent shift is dominated by effects arising from the structure of the second coordination shell, we seek ways of improving the accuracy of the calculation.

The simplest method available for the inclusion of nonrigidity is to expand the intramolecular potential of the $Fe^{2+}(H_2O)_6$ complex in terms of a local quadratic force field, e.g., potential TF2. As can be seen from Figure 6, the resulting radial and angular distribution functions reproduce those obtained using the full potential TF1 very well. Interestingly, inclusion of just the radial component of the intramolecular potential by itself allows insufficient relaxation to correctly reproduce the radial distribution function, and it is essential to represent adequately the angular components of the potential surface. Here, for testing purposes, we designed potential TF2 to mimic Tomasi's potential TF1, but in general such an intramolecular surface could be determined using conventional quantum mechanical techniques, allowing the effects of floppiness of the complex to be included, if necessary.

The calculated solvent shift of the localized MLCT transition derived from these simulations is shown in Figure 7 as a function of the cavity radius a. The TR/SM simulation predicts $\Delta\nu = -1990$ cm^{-1}, only 10% larger than the value -1810 cm^{-1} obtained from the reference simulation, TF1/SM. As anticipated, this difference arises primarily due to contributions from water molecules in the second coordination shell, up to $a = 6$ Å. The results show that rigidity of the inner shell has no dominant influence on the total solvent shift. Inclusion of corrections for the flexibility of the inner shell, as is done in potential TF2, removes most of the calculated discrepancy, the calculated solvent shift being -1760 cm^{-1}.

(d) Use of Simple Methods to Generate the Potential Surface. Results from our EF/SM simulations are shown in Figure 6, along with the results previously described obtained using Tomasi's potential TF1/SM. In general, the results are encouragingly similar, but significant differences are seen for g_{Fe-O} in the second coordination shell. Each potential predicts that 12 water molecules lie in this shell, as observed,[26] but our

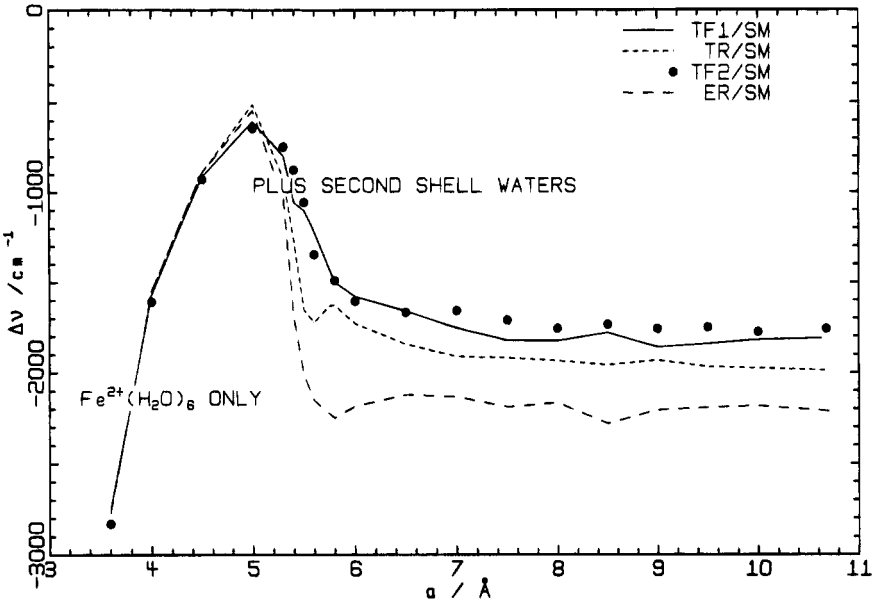

Figure 7. MLCT solvent shift $\Delta\nu$ is shown as a function of the outer cavity radius $a = r + r_x$ (at exclusion radius $r_x = 1.001$ Å) obtained using the smoothing function SM and four different potential surfaces: TF1, Tomasi's potential, flexible inner shell; TR, Tomasi's potential for outer-shell interactions with a rigid inner shell; TF2, Tomasi's potential for outer-shell interactions with a force field for the inner-shell interactions; and ER, our ESP-derived potential for the outer-shell interactions with a rigid inner shell.

potential predicts that this shell is considerably more structured, with a larger peak and much deeper subsequent trough. The difference in the structure can be attributed to the differences in the water−water interactions between the first and second shells: in potential TF1, bulk water charges are used to describe the potential of the inner shell waters, but in EF this constraint is lifted and much larger atomic charges result as a consequence of charge transfer and polarization of the ligands by the ion. These increased atomic charges produce stronger intermolecular interactions between the water shells. Insufficient experimental data is available to discriminate between these two potential surfaces; if the *ab initio* calculations correctly describe the charge transfer and polarization effects, then the EF potential would naively be expected to give the most reliable results. Perhaps an improved potential surface could be generated by including the ion and its ligands inside a dielectric cavity during the *ab initio* SCF calculations.[45]

The calculation ER/SM differs from EF/SM in that the ligands are held rigid. No large effects on the solvent structure around the complex are seen, and the results are not described in detail. As for Tomasi's potential, the most significant effect is increase of the height of the maximum of g_{Fe-O} for the second coordination shell by ca. 0.5; the depth of the minimum past the second shell is not significantly affected, and there are no long-range effects.

The calculated MLCT solvent shifts for the ER/SM and EF/SM simulations are essentially equal, indicating that inner-shell nonrigidity is not a critical condition. Results for ER/SM are shown in Figure 7 along with results previously described for Tomasi's potential. An increase in the magnitude of the solvent shift of 400 cm^{-1} is seen after $a = 5$ Å, attributable to the increased structuring of the second coordination shell. Clearly, the best possible representation of the second shell is essential in order to obtain an accurate description of the solvent shift in MLCT transitions.

IV. Mechanistic Implications

(a) Direct MLCT Absorption (Mechanism 1). Electronic structure calculations for the $Fe^{2+}(H_2O)_6$ complex have been performed in order to determine the gas-phase (T_h symmetry) transition energy and oscillator strength for the MLCT absorption band using both INDO/S-CI and *ab initio* techniques. The INDO/S-CI calculations are performed using the rotationally invariant[128] spin-restricted open-shell[135] (ROHF) formalism with configuration interaction developed by Zerner[128,135-138] using our own software. (Technically, the free Fe atom is represented by its d^7s^1 configuration,[137] a single-ζ basis set comprising[128] contracted Slater functions is used for the d orbitals, Mataga−Nishimoto−Weiss[136] two-electron integrals are used, and the one-electron interaction factors[136] are set to $f_{pp,\sigma} = 1.267$, $f_{pp,\pi} = 0.585$, and $f_{ss,\sigma} = f_{dd,\sigma} = f_{dd,\pi} = f_{dd,\delta} = 1$.) All possible excitations amongst an active space of the metal 3d and 4s orbitals are included in the configuration interaction calculation,[138] as are a large number of single excitations from each of those configurations. The result is a predicted weak gas-phase delocalized MLCT transition at $\nu = 71\,000$ cm^{-1} (8.8 eV) with an oscillator strength of 0.012. All-electron *ab initio* calculations, performed by the MOLCAS program[139] and a complete active space SCF (CASSCF) technique using a STO-3G basis set for water and a triple-ζ basis set for iron,[140] coincidently predict the same frequency, $\nu = 71\,000$ cm^{-1} (8.8 eV). If the MLCT remains delocalized over all six ligands, then little solvent shift is expected; possible localization of the transition on one of the ligands would be associated with a small energy lowering and also a solvent shift of at most ca. −2000 cm^{-1} (0.25 eV), as calculated in section III. Figure 8 shows the observed absorption band, together with an arrow at 69 000 cm^{-1} (8.6 eV), indicating the calculated lowest possible energy for the band center. It is thus highly unlikely that this transition could have a significant influence on the absorption spectrum in the region 40 000−50 000 cm^{-1} (5−6 eV); for this to be the case, the observed intensity in that region ($f = 0.0011$) would need to comprise about 10% of that ($f = 0.012$) predicted for the MLCT band.

(b) Absorption of a d → s Nature (Mechanism 2). INDO/S-CI calculations predict that the ^5S transition observed[124] in the free ion at 41 000 cm^{-1} is blue shifted to 50 000 cm^{-1} (6.2 eV) in the hexaaquo complex. Similarly, *ab initio* multiconfigurational SCF (MCSCF) calculations (the active space being all single and double excitations from the iron d orbitals into the lowest 15 virtual orbitals) performed using the basis sets and programs described in section II predict an absorption

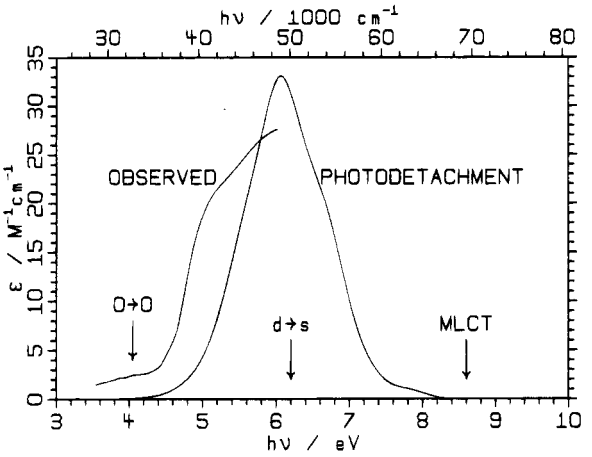

Figure 8. Observed[66] absorption spectrum of aqueous $Fe^{2+}(H_2O)_6$ compared to the spectrum calculated for photodetachment of an electron into a preexisting solvent cavity (at 0.1 eV resolution). The 0—0 transition energy, calculated from experimental data in section I, and the band centers calculated for 3d → 4s and MLCT absorptions are indicated with arrows.

frequency of 51 000 cm^{-1} (6.3 eV). It is difficult to estimate error bounds for these numbers, but general experience would suggest that 4000 cm^{-1} (0.5 eV) would be an upper limit, with the true frequency probably lying to lower energy. This places the d → s transition well within the observed absorption band (see Figure 8), and it is possible that it significantly inhibits (e.g., by not leading to electron release, thus reducing the observed quantum yield), aids (i.e., leads eventually to electron release), or facilitates (i.e., is the sole mechanism which leads to electron release) the photochemical reaction.

(c) Direct Photodetachment (Mechanism 4). The spectrum calculated using the method described in section IIe, smoothed using Gaussian convolution at a resolution of 0.1 eV, is shown in Figure 8 along with the observed spectrum.[66] The calculated band is centered at 6.0 eV (48 000 cm^{-1}) and has an oscillator strength of 0.0017; its foot is at 4.5 eV, slightly above the energy of 4.0 eV calculated from experimental data in section I for the enthalpy difference between the ground state and the fully equilibrated excited state. These results do indeed suggest that direct photodetachment is the primary absorption process. Note, however, that the quality of the agreement seen between theory and experiment in Figure 8 is beyond that which could reasonably be expected given the approximations used in generating the spectra. A 5% error, for example, in the calculated average solvent shift of 29.7 eV would produce a 1.5 eV error in the band position, and the approximation used do describe the kinetic energy, eq 8, is likely accurate to say ±0.5 eV. Similarly, the intensities derived from the rather arbitrary assumptions used in deriving (11) could easily be in error by 1 order of magnitude. Further, the observed absorption band, based on the spectra of other ions,[68] could possibly continue to rise to a maximum of ca. $\epsilon = 500$ M^{-1} cm^{-1} at ν = ca. 7 eV, making the contribution attributed here to direct photodetachment of only minor significance. Nevertheless, the observed part of the absorption spectrum is qualitatively well represented, and any large absorption at higher frequency than that observed could be attributable to a different mechanism.

An analysis of all of the solvent cavities found in the liquid structure shows that the cavity to water radial distribution functions reproduce in detail those found in pure water.[78] In a sample as large as ours, most cavities lie outside the second coordination shell. Our transition moment profile, however, contains an orbital overlap term which decreases exponentially with the distance of the cavity from the ion, effectively precluding transitions to cavities located outside of the second

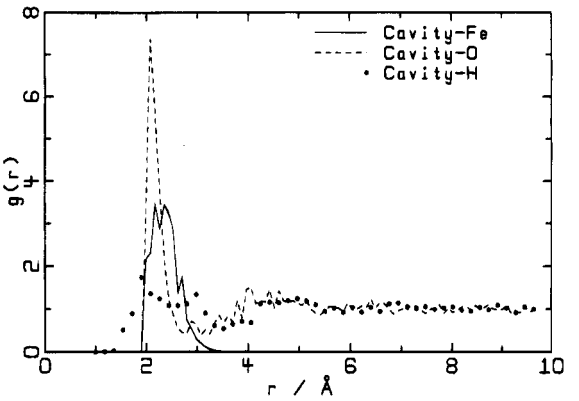

Figure 9. Preexisting cavity center to atom radial distribution functions, weighted according to the calculated oscillator strength of the metal to cavity (photodetachment) transition.

shell. The cavities between the first and second shells have different structures to the cavities in the bulk liquid (i.e., those outside of the second shell), and the cavity—atom radial distribution functions, weighted by the oscillator strength of the transition to the cavity, are shown in Figure 9. The oxygen—cavity function is abruptly truncated at 2 Å due to the hard-sphere potential used for the exchange repulsion terms. It has a deep trough near 3 Å, and four water molecules span each cavity which is centrally located with respect to those water molecules. The iron—cavity function decreases rapidly near 2 Å as shorter distances bring the center too close to an oxygen atom; the average separation is 2.5 Å, providing the electron with a small direct coupling to the ion through the (111) "hole" between the ligands. The average kinetic energy of the electron and solvent shift are calculated to be 5.2 and −29.7 eV, respectively.

V. Conclusions

We have outlined a development of our methods, parts I—III,[1-3] for estimating solvent shifts of electronic spectra for species with strong specific solvent—solute interactions (e.g., hydrogen bonds) to treat inorganic charge transfer spectra. The specific first application has been to the ultraviolet absorption spectrum of aqueous $Fe^{2+}(H_2O)_6$, an interesting problem which has remained unexplained for over 60 years. Our calculations predict that direct photodetachment (mechanism 4) will give rise to an absorption band of essentially the same frequency, intensity, and bandwidth as is experimentally observed. They also indicate that processes involving direct MLCT absorption (mechanism 1) do not contribute significantly to the observed photochemical process for this complex and that the frequency of the formally forbidden d → s transition (mechanism 2) is close to that observed, but estimation of the magnitude of any contribution which this may make requires a knowledge of the relevant intensity-gaining mechanism, which is as yet unknown. The question of any possible contribution of the CTTS mechanism (mechanism 3) to the photochemical process must await developments in computer technology in order for a reliable calculation to be made. Such a calculation would need to treat fully quantum mechanically at least the metal 3d, 4s, and 4p orbitals, MLCT states, and direct photodetachment states as well as the solvent polarization borne CTTS states.

Our calculations indicate that, for metal-containing systems, no one single mechanism is likely to be generally applicable to describe photochemical water decomposition. Indeed, all four mechanisms considered herein could in principle dominate in any given specific situation. This qualitatively explains the widely varying oscillator strengths observed for photochemically active bands for metallic complexes. Experimentally, absorption

spectra (for example, see ref 68) need to be determined to high enough energy to properly characterize the band shape (into the vacuum-ultraviolet region if necessary, e.g., for $Fe^{2+}(H_2O)_6$). Also, femtosecond dynamical studies[87,92] of the motion of the excitation and/or electroabsorption spectroscopic studies[141,142] (which allows excited state dipole moments and polarizabilities to be determined,[6,7,143] thus characterizing the excited state) should be performed.

Our method for evaluating solvent shifts in strongly interacting systems is seen to be highly robust and capable of describing very different physical situations with quantitative accuracy. Previously, the method was tested by calculation of hydrogen-bonding blue shifts in azines line pyridine[12] and pyrimidine[3] where the solvent shift is ca. 0.25 eV. There, contributions from specific solvation and dielectric effects are of equal importance and of the same sign. Here, for a MLCT process in which the donor and acceptor lie in the same solvent hole and the ground state has no dipole moment, a similarly low solvent shift is predicted, but in this case the specific solvation and dielectric effects oppose each other. At present, we are investigating[144] the MLCT solvent shift in $Ru^{2+}(NH_3)_5$pyridine, in which the ground state has a large charge asymmetry; this produces a sizeable red shift of ca. 1 eV, quantitatively in agreement with experiment. Finally, in this work in what is an extreme limit, we investigate a photodetachment process in which the electron goes into a solvent cavity and the donor and acceptor states of the charge transfer process must be thought of as residing in different solvent cavities. Regardless of whether the intensity calculation presented is accurate or not (i.e., whether mechanism 4 is or is not the major mechanism involved), the calculation of a solvent shift of ca. −30 eV must be quite accurate, as the gas-phase transition energy and the origin of any possible absorption band are both known precisely, and only the minor contribution from the electron kinetic energy is uncertain. Our general method is thus expected to be generally applicable to a wide range of problems.

Simulating charged systems is not straightforward due to the long-range nature of the Coulombic potential and the impracticality of using sample sizes whose extent exceeds its range. A key feature of the solvent shift for complexes like this with no dipole moment in the initial state is found to be that it is dominated by interactions with the second coordination shell and is relatively insensitive to long-range interactions. Solvent shifts calculated using relatively small sample sizes are thus expected to be reliable, and computationally efficient boundary conditions such as ST may be used. This may not be the case however if the initial state has a large dipole moment, as then a large contribution to the solvent shift arises from the orientational contributions to the dielectric constant in eq 14, and the solvent shift would contain terms of the form of eq 12, which are long-range in nature.

We have also shown that it is not necessary to model the structure of the inner coordination shell to high accuracy in order to determine the MLCT solvent shift. Complexes like $Fe^{2+}(H_2O)_6$ are less strongly bound than many other transition metal complexes, and hence their structure could be expected to be anomalously flexible. Even for this complex, errors only on the order of 10% are introduced by holding the inner shell rigid, and simple correction techniques such as the inclusion of a harmonic intramolecular force field adequately describe the deviations from rigidity. It appears to be considerably more important to describe the second coordination shell as accurately as possible. Significant differences in the solvent shift are predicted depending upon whether potentials describing on an equal footing the interactions within the complex and between the complex and the solvent, or which use separate intermolecular and intramolecular potentials, are used. Combining these results, it appears that simple calculations which hold the inner shell rigid and determine only interactions of the complex with the solvent provide the most economical and most accurate method for determining solvent shifts.

Acknowledgment. J.Z., J.S.C., and J.R.R. gratefully acknowledge support provided by the Australian Research Council for this project. We thank Dr. D. E. Smith, Pacific Northwest Laboratories, for helpful discussions and advice concerning the use of various boundary conditions.

The following registry numbers were supplied by the author: $Fe^{2+}(H_2O)_6$ 15365-81-8; $Fe^{3+}(H_2O)_6$ 15377-81-8; $V^{2+}(H_2O)_6$ 15696-18-1; $Cr^{2+}(H_2O)_6$ 20574-26-9; $Ru^{2+}(NH_3)_6$ 19652-44-9; $[Fe(CN)_6]^{4-}$ 13408-63-8.

References and Notes

(1) Zeng, J.; Craw, J. S.; Hush, N. S.; Reimers, J. R. *J. Chem. Phys.* **1993**, *99*, 1482.
(2) Zeng, J.; Hush, N. S.; Reimers, J. R. *J. Chem. Phys.* **1993**, *99*, 1495.
(3) Zeng, J.; Hush, N. S.; Reimers, J. R. *J. Chem. Phys.* **1993**, *99*, 1508.
(4) Reimers, J. R.; Hush, N. S. *Inorg. Chem.* **1990**, *29*, 3686.
(5) Reimers, J. R.; Hush, N. S. *Inorg. Chem.* **1990**, *29*, 4510.
(6) Reimers, J. R.; Hush, N. S. In *Mixed Valence Systems: Applications in Chemistry, Physics, and Biology*; Prassides, K., Ed.; Kluwer Academic Publishers: Dordrecht, 1991; p 29.
(7) Reimers, J. R.; Hush, N. S. *J. Phys. Chem.* **1991**, *95*, 9773.
(8) Hush, N. S.; Paddon-Row, M. N.; Cotsaris, E.; Oevering, H.; Verhoeven, J. W.; Heppener, M. *Chem. Phys. Lett.* **1985**, *117*, 8.
(9) Reimers, J. R.; Hush, N. S. *Chem. Phys.* **1990**, *146*, 105.
(10) Reimers, J. R.; Hush, N. S.; Sameth, D.; Callis, P. R. *Chem. Phys. Lett.* **1990**, *169*, 622.
(11) Mikkelsen, K. V.; Ratner, M. A. *Chem. Rev.* **1987**, *87*, 113.
(12) Zeng, J.; Craw, J. S.; Hush, N. S.; Reimers, J. R. *Chem. Phys. Lett.* **1993**, *206*, 318.
(13) Kirkwood, J. G. *J. Chem. Phys.* **1934**, *2*, 351.
(14) Onsager, L. *J. Am. Chem. Soc.* **1936**, *58*, 1486.
(15) McRae, E. G. *J. Phys. Chem.* **1957**, *61*, 562.
(16) Bayliss, N. S. *J. Chem. Phys.* **1950**, *18*, 292.
(17) Levich, V. G. In *Physical Chemistry an Advanced Treatise IX*; Eyring, H., Ed.; Academic: New York, 1970; p 985.
(18) Liptay, W. In *Modern quantum chemistry;* Sinanoglu, O., Ed.; Academic Press: New York, 1965; Vol. III, p 45.
(19) Rettig, W. *J. Mol. Struct.* **1982**, *84*, 303.
(20) Karelson, M. M.; Zerner, M. C. *J. Am. Chem. Soc.* **1990**, *112*, 9405.
(21) Mikkelsen, K. V.; Agren, H.; Jensen, H. J. Aa.; Helgaker, T. *J. Chem. Phys.* **1988**, *89*, 3086.
(22) Agren, H.; Knuts, S.; Mikkelsen, K. V.; Jensen, H. J. Aa. *Chem. Phys.* **1992**, *159*, 211.
(23) Agren, H.; Mikkelsen, K. V. *J. Mol. Struct.* **1991**, *234*, 425.
(24) Tomasi, J.; Bonaccorsi, R.; Cammi, R.; Olivares del Valle, F. J. *J. Mol. Struct.* **1991**, *234*, 401.
(25) Luzhkov, V.; Warshel, A. *J. Am. Chem. Soc.* **1991**, *113*, 4491.
(26) Ohtaki, H.; Radnai, T. *Chem. Rev.* **1993**, *93*, 1157.
(27) Brooks, C. L.; Pettitt, B. M.; Karplus, M. *J. Chem. Phys.* **1985**, *83*, 5897.
(28) Brooks, C. L. *J. Chem. Phys.* **1987**, *87*, 3029.
(29) Linse, P.; Andersen, H. C. *J. Chem. Phys.* **1986**, *85*, 3027.
(30) Madura, J. D.; Pettitt, B. M. *Chem. Phys. Lett.* **1988**, *150*, 105.
(31) Ewald, P. P. *Ann. Phys.* **1921**, *64*, 253.
(32) Barker, J. A.; Watts, R. O. *Mol. Phys.* **1973**, *26*, 789.
(33) Clementi, E. *Modern Techniques in Computational Chemistry (MOTECC)*; Escom: Leidon, 1990.
(34) Corongiu, G.; Clementi, E. *J. Chem. Phys.* **1978**, *69*, 4885.
(35) Cossi, M.; Persico, M. *Theor. Chim. Acta* **1991**, *81*, 157.
(36) Curtiss, L. A.; Halley, J. W.; Hautman, J.; Rahman, A. *J. Chem. Phys.* **1987**, *86*, 2319.
(37) Cordeiro, M. N. D. S.; Gomes, J. A. N. F.; Gonzàlez-Lafont, A.; Lluch, J. M.; Bertrán, J. *Chem. Phys.* **1990**, *141*, 379.
(38) Rode, B. M.; Islam, S. M. *Z. Naturforsch., Teil A* **1991**, *46*, 357.
(39) Curtiss, L. A.; Halley, J. W.; Hautman, J. *Chem. Phys.* **1989**, *133*, 89.
(40) Curtiss, J. A.; Jurgens, R. *J. Phys. Chem.* **1990**, *94*, 5509.
(41) Floris, F.; Persico, M.; Tani, A.; Tomasi, J. *Chem. Phys. Lett.* **1992**, *199*, 518.
(42) Astrand, P.-O.; Wallqvist, A.; Karlstrom, G.; Linse, P. *J. Chem. Phys.* **1991**, *93*, 8419.
(43) Cadwell, J.; Dang, L. X.; Kollman, P. A. *J. Am. Chem. Soc.* **1990**, *112*, 9144.

(44) Cieplak, P.; Kollman, P. A. *J. Chem. Phys.* **1990**, *92*, 6761.
(45) Pappalardo, R. R.; Marcos, E. S. *J. Phys. Chem.* **1993**, *97*, 4500.
(46) Weiner, S. J.; Kollman, P. A.; Case, D. A.; Singh, U. C.; Ghio, C.; Alagona, G.; Profeta, S., Jr.; Weiner, P. *J. Am. Chem. Soc.* **1984**, *106*, 765.
(47) Weiner, S. J.; Kollman, P. A.; Nguyen, D. T.; Case, D. A. *J. Comput. Chem.* **1986**, *7*, 230.
(48) Balzani, V.; Scandola, F. *Supramolecular Photochemistry*; London: Ellis Horwood, 1991.
(49) Broo, A.; Larsson, S. *Chem. Phys.* **1992**, *161*, 363.
(50) Broo, A. *Chem. Phys.* **1993**, *174*, 127.
(51) Brunschwig, B. S.; Creutz, C.; Macartney, D. H.; Sham, T.-K.; Sutin, N. *Faraday Disuss. Chem. Soc.* **1982**, *74*, 113.
(52) Merbach, A. E.; Akitt, J. W. In *NMR Basic Principles and Progress*; Diehl, P., Ed.; Springer: Berlin, 1991; Vol. 24, p 129.
(53) Gonzàlez-Lafont, A.; Lluch, J. M.; Oliva, A.; Bertrán, J. *Chem. Phys.* **1987**, *111*, 241.
(54) Guàrdia, E.; Padró, J. A. *Chem. Phys.* **1990**, *144*, 353.
(55) Berendsen, H. J.; Postma, J. P. M.; van Gunsteren, W. F.; Hermans, J. In *Intermolecular Force*; Pullman, B., Ed.; Reidel: Dordrecht, 1981.
(56) Toukan, K.; Rahman, A. *Phys. Rev.* **1985**, *B31*, 2643.
(57) Best, S. P.; Forsyth, J. B. *J. Chem. Soc., Dalton Trans.* **1990**, 395.
(58) Figgis, B. N.; Kucharski, E. S.; Reynolds, P. A. *Acta Crystallogr.* **1989**, *C45*, 942.
(59) Jafri, J. A.; Logan, J.; Newton, M. D. *Isr. J. Chem.* **1980**, *19*, 340.
(60) Knerfel, C. L.; Friedman, H. L.; Newton, M. D. *Z. Naturforsch.* **1989**, *44a*, 385.
(61) Kuharski, R. A.; Bader, J. S.; Chandler, D.; Sprik, M.; Klein, M. L.; Impey, R. W. *J. Chem. Phys.* **1988**, *89*, 3248.
(62) Bader, J. S.; Kuharski, R. A.; Chandler, D. *J. Chem. Phys.*, **1990**, *93*, 230.
(63) Potteril, R. H.; Walker, O. J.; Weiss, J. *Proc. R. Soc. (London)* **1936**, *A156*, 561.
(64) Weiss, J. *Trans. Faraday Soc.* **1941**, *37*, 463.
(65) Farkas, A.; Farkas, L. *Trans. Faraday Soc.* **1938**, *34*, 1113.
(66) Rigg, T.; Weiss, J. *J. Chem. Phys.* **1952**, *20*, 1194.
(67) Hayon, E.; Weiss, J. *J. Chem. Soc.* **1960**, 3866.
(68) Dainton, F. S.; James, D. G. L. *Trans. Faraday Soc.* **1958**, *54*, 649.
(69) Orgel, L. E. *J. Chem. Phys.* **1955**, *23*, 1004.
(70) Jorgensen, C. K. *Acta Chem. Scand.* **1955**, *9*, 919.
(71) Orgel, L. E. *Disc. Institutes Solvay* **1956**, *10*, 289.
(72) Jortner, J.; Stein, G. *J. Phys. Chem.* **1962**, *66*, 1264.
(73) Dainton, F. S.; Jones, F. T. *Trans. Faraday Soc.* **1965**, *61*, 1681.
(74) Airy, P. L.; Dainton, F. S. *Proc. R. Soc. (London)* **1966**, *A291*, 340.
(75) Sloper, R. W.; Braterman, P. S.; Cairns-Smith, A. G.; Truscott, T. G.; Craw, M. *J. Chem. Soc., Chem. Commun.* **1983**, 488.
(76) Matsubara, T.; Efrima, S.; Metiu, H. I.; Ford, P. C. *J. Chem. Soc., Faraday Trans. 2* **1979**, *75*, 390.
(77) Blandamer, M. J.; Fox, M. F. *Chem. Rev.* **1970**, *70*, 59.
(78) Schnitker, J.; Rossky, P. J.; Kenney-Wallace, G. A. *J. Chem. Phys.* **1986**, *85*, 2986.
(79) Alfano, J. C.; Walhout, P. K.; Kimura, Y.; Barbara, P. F. *J. Chem. Phys.* **1993**, *98*, 5996.
(80) Jortner, J.; Stein, G. *J. Phys. Chem.* **1962**, *66*, 1258 .
(81) Lu, H.; Long, F. H.; Bowman, R. B.; Eisenthal, K. B. *J. Phys. Chem.* **1989**, *93*, 27.
(82) Holmes, O. G.; McClure, D. S. *J. Chem. Phys.* **1957**, *26*, 1686.
(83) Balzani, V.; Carassiti, V. *Photochemistry of Coordination Compounds*; Academic Press: London, 1970.
(84) Nikogosyan, D. N.; Oraevsky, A. A.; Rupasov, V. I. *Chem. Phys.* **1983**, *77*, 131.
(85) Migus, A.; Gaudel, Y.; Martin, J. L.; Antonetti, A. *Phys. Rev. Lett.* **1987**, *58*, 1559.
(86) Rossky, P. J.; Schnitker, J. *J. Phys. Chem.* **1988**, *92*, 4277.
(87) Long, F. H.; Lu, H.; Eisenthal, K. B. *Phys. Rev. Lett.* **1990**, *64*, 1469.
(88) Murphrey, T. H.; Rossky, P. J. *J. Chem. Phys.* **1993**, *99*, 515.
(89) Bowman, R. M.; Lu, H.; Eisenthal, K. B. *J. Chem. Phys.* **1988**, *89*, 606.
(90) Stein, G.; Treinin, A. *Trans. Faraday Soc.* **1959**, *55*, 1086.
(91) Jortner, J.; Ottolenghi, M.; Stein, G. *J. Phys. Chem.* **1964**, *68*, 247.
(92) Long, F. H.; Lu, H.; Shi, X.; Eisenthal, K. B. *Chem. Phys. Lett.* **1990**, *169*, 165.
(93) Sheu, W.-S.; Rossky, P. *J. Am. Chem. Soc.* **1993**, *115*, 7729.
(94) Sheu, W.-S.; Rossky, P. *Chem. Phys. Lett.* **1993**, *202*, 186.
(95) Sheu, W.-S.; Rossky, P. *Chem. Phys. Lett.* **1993**, *213*, 233.
(96) Truong, T. B. *J. Chem. Phys.* **1981**, *74*, 3561.
(97) Gray, H. B.; Beach, N. A. *J. Am. Chem. Soc.* **1963**, *85*, 2922.
(98) Alexander, J. J.; Gray, H. B. *Coord. Chem. Rev.* **1967**, *2*, 29.
(99) Horvàth, A.; Uzonyi, Z. S. *Inorg. Chim. Acta*, **1990**, *170*, 1.
(100) Kunkely, H.; Vogler, A. *J. Organomet. Chem.* **1992**, *431*, C42.
(101) Bard, A. J.; Parsons, R.; Jordan, J., Eds. *Standard potentials in aqueous solution*; Marcel Dekker: New York, 1985.
(102) Hart, E. J.; Aubar, M. *The hydrated electron*; Wiley-Interscience: New York, 1970; p 62.
(103) Jortner, J.; Noyes, R. M. *J. Phys. Chem.* **1966**, *70*, 770.
(104) McDonald, I. R. *Mol. Phys.* **1972**, *23*, 41.
(105) Metropolis, N. A.; Rosenbluth, A. W.; Rosenbluth, M. N.; Teller, A. H.; Teller, E. *J. Chem. Phys.* **1953**, *21*, 1087.
(106) Wood, W. W.; Parker, F. R. *J. Chem. Phys.* **1957**, *27*, 720.
(107) Kincaid, R. H.; Scheraga, H. A. *J. Comput. Chem.* **1982**, *3*, 525.
(108) Alper, H. E.; Levy, R. M. *J. Chem. Phys.* **1989**, *91*, 1242.
(109) Adams, D. J. *Chem. Phys. Lett.* **1979**, *62*, 329.
(110) Adelman, S. A. *J. Chem. Phys.* **1980**, *73*, 3145.
(111) Allen, M. P.; Tildesley, D. J. *Computer Simulation of Liquids*; Clarendon: Oxford, 1987.
(112) Smith, W.; Fincham, D. *Mol. Simul.* **1993**, *10*, 67.
(113) Smith, D. E.; Haymet, A. D. J. *J. Chem. Phys.* **1993**, *98*, 6445.
(114) Hansen, J. P. *Phys. Rev. A* **1973**, *8*, 3096.
(115) Heyes, D. M. *J. Chem. Phys.* **1980**, *74*, 1924.
(116) Smith, P. E.; Pettitt, B. M. *J. Am. Chem. Soc.* **1991**, *113*, 6029.
(117) Dolg, M.; Wedig, U.; Stoll, H.; Preuss, H. *J. Chem. Phys.* **1987**, *86*, 866.
(118) Preuss, H.; Stoll, H.; Wedig, U.; Kruger, Th. *Int. J. Quantum Chem.* **1981**, *19*, 113.
(119) Hay, T. H. Dunning, Jr.; Hay, P. J. In *Modern Theoretical Chemistry*; Schaefer, H. F., III, Ed.; Plenum: New York, Vol. 3, 1976.
(120) Dupuis, M.; Rys, J.; King, H. F. *J. Chem. Phys.* **1976**, *65*, 111.
(121) Eisenberg, D.; Kauzmann, W. *The Structure and Properties of Water*; Oxford: Oxford, 1969.
(122) Weast, R. C., Ed. *Handbook of Chemistry and Physics, 55th ed.*; Chemical Rubber Company: Cleveland, 1974.
(123) Marcos, E. S.; Pappalardo, R. R.; Rinaldi, D. *J. Phys. Chem.* **1991**, *95*, 8928.
(124) Moore, C. E. *Atomic Energy Levels;* National Bureau of Standards Circ. 467; Washington, DC, 1958.
(125) Schnitker, J.; Rossky, P. J. *J. Chem. Phys.* **1987**, *86*, 3471.
(126) Wallqvist, A.; Martyna, G.; Berne, B. J. *J. Phys. Chem.* **1988**, *92*, 1721.
(127) Schnitker, J.; Rossky, P. *J. Chem. Phys.* **1987**, *86*, 3462.
(128) Bacon, A. D.; Zerner, M. C. *Theor. Chim. Acta* **1979**, *53*, 21.
(129) Zerner, M. C. ZINDO Quantum Chemistry Package, University of Florida, Gainesville, FL.
(130) Pople, J. A.; Beveridge, D. L. *Approximate Molecular Orbital Theory*; McGraw-Hill: New York, 1970.
(131) Best, S. P.; Forsyth, J. B.; Tregenna-Piggott, P. L. *J. Chem. Soc., Dalton Trans.* **1993**, 1.
(132) Herdman, G. J.; Neilson, G. W. *J. Phys.: Condens. Matter* **1992**, *4*, 649.
(133) Enderby, J. E.; Cummings, S.; Herdman, G. J.; Neilson, G. W.; Salmon, P. S.; Skipper, N. *J. Phys. Chem.* **1987**, *91*, 5851.
(134) Kasha, M. *Disc. Faraday Soc.* **1950**, *9*, 14.
(135) Edwards, W. D.; Zerner, M. C. *Theor. Chim. Acta* **1987**, *72*, 347.
(136) Ridley, J. E.; Zerner, M. C. *Theor. Chim. Acta* **1973**, *32*, 111.
(137) Zerner, M. C.; Loew, G. H.; Kirchner, R. F.; Mueller-Westerhoff, U. T. *J. Am. Chem. Soc.* **1980**, *102*, 589.
(138) Anderson, W. P.; Edwards, W. D.; Zerner, M. C. *Inorg. Chem.* **1986**, *25*, 2728.
(139) Andersson, K.; Füscher, M. P.; Lindh, R.; Malmqvist, P.-A.; Olsen, J.; Roos, B. O.; Sadlej, A. J.; Widmark, P. O. University of Lund, Sweden.
(140) Wachters, A. J. H. *J. Chem. Phys.* **1970**, *52*, 1033.
(141) Lockhart, D. J.; Goldstein, R. F.; Boxer, S. G. *J. Chem. Phys.* **1988**, *89*, 1408.
(142) Oh, D. H.; Sano, M.; Boxer, S. G. *J. Am. Chem. Soc.* **1991**, *113*, 6880.
(143) Liptay, W. *Z. Naturforsch. Teil. A* **1965**, *20*, 272.
(144) Zeng, J.; Hush, N. S.; Reimers, J. R. In preparation.